Earth, Planets and Space
a SpringerOpen Journal

LETTER Open Access

Sub-seafloor resistivity sensing using a vertical electrode configuration

Takumi Ueda[1*], Yuji Mitsuhata[1], Motoharu Jinguji[1] and Hisatoshi Baba[2]

Abstract

There is growing interest in marine direct current (DC) resistivity methods for sub-seafloor exploration of a broad range of geophysical and geological targets. To address this, we have developed a new marine DC method with a vertical electrode configuration (VEC). Compared to conventional marine DC methods that use a horizontal electrode configuration, the shape and position of our VEC cable can be controlled relatively easily. Therefore, the VEC is suitable for operations in regions of steep bathymetry and for expeditious sub-seafloor resistivity exploration. In this study, we introduce a water-resistant electrode array cable and an onshore multichannel DC measurement system for stable and rapid data acquisition. To evaluate the performance and efficiency of the new system, we conducted field experiments in the shallow water zone at Shimizu Port, Suruga Bay, Japan. In order to quantitatively analyze the VEC-DC data, we adopt a 1-D numerical modeling code that computes the electric potential and apparent resistivity generated by a point and dipole current source used in the VEC-DC measurement. These can be placed at any position with an arbitrary electrode configuration in a multilayered space, including seawater and sub-seafloor layers. We also develop an inversion code for the VEC-DC data based on a simulated annealing (SA) optimization and applied this to the field data. The observed data is of sufficiently good quality to be used for inversion, and the SA result demonstrates that the proposed VEC-DC system is able to estimate the sub-seafloor resistivity structure.

Keywords: Direct current method; Vertical electrode configuration; Marine exploration; Seafloor resistivity

Findings

Introduction

The use of marine (offshore) and underwater electromagnetic (EM) and direct current (DC) exploration methods for various geological and engineering targets has generated considerable interest in recent years (e.g., Constable 2010; Edwards et al. 1985; Goto et al. 2008; Holten et al. 2009; Loke and Lane 2004; Orlando 2013). Typical targets for marine EM and DC methods include port facilities, active fault structures, groundwater conditions, nuclear waste depository sites, carbon dioxide capture and storage, hydrocarbon reservoirs, and seafloor hydrothermal deposits beneath coastal and deep-water areas. To address these social demands, it is important to develop appropriate survey methods according to the local conditions, such as the depth of the targets and seawater.

In this study, we develop a new marine DC method with a vertical electrode configuration (VEC) (e.g., Baumgartner 1996; Barsukov et al. 2007; Holten et al. 2009). The basic theory and concept of our marine VEC-DC method are based on standard onshore (e.g., Reynolds 1997; Zhdanov and Keller 1994) and offshore/underwater (e.g., Chave et al. 1991) DC methods. The difference between conventional onshore and marine DC methods is that the proposed VEC-DC method measures electric potentials using vertically deployed electrodes. Compared to the conventional horizontal electrode configuration, the shape and position of the electrode cable in the VEC can be controlled relatively easily, without the need for positioning equipment such as an acoustic pinger. Therefore, the VEC-DC is suitable for exploration in regions of steep bathymetry and could become the preferred method for surveying shallow sub-seafloor targets in both coastal and deep water areas. In this study, we focus on the instrumentation required for data acquisition and the numerical analysis of VEC-DC data. In terms of instrumentation, we have introduced a water-resistant electrode array cable

*Correspondence: takumi.ueda@aist.go.jp
[1]Geological Survey of Japan, AIST, Central 7, 1-1-1, Higashi, Tsukuba 305-8567, Japan
Full list of author information is available at the end of the article

and an onshore multichannel DC survey system. These will improve the data quality compared to that collected during preliminary feasibility experiments.

A series of field tests were conducted using our new system in the shallow water zone at Shimizu Port, Suruga Bay, Japan. To evaluate and interpret the field data, the computation of theoretical responses (forward modeling) is essential, as is data inversion for a layered earth including seawater layers. We apply theoretical formulas presented in Mitsuhata and Ueda (2010) and Ueda et al. (2010) using the process of recursive relations introduced by Sato (2000) to calculate the electric potential generated by a point and/or dipole current source placed at any position in a multilayered space. Based on these theoretical formulas, we implement a numerical calculation tool to compute the electric potentials in Ueda et al. (2010). Moreover, we develop an inversion method for the VEC-DC data using simulated annealing (SA) optimization (e.g., Sen et al. 1993; Sharma 2012). Finally, we perform a numerical analysis of the observed data based on the electric potential calculation and SA inversion.

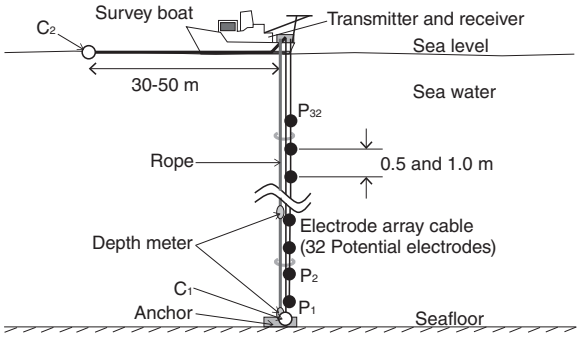

Figure 2 Measurement configuration. Measurement configuration of the proposed marine VEC-DC method with two current electrodes (C_1 at the seafloor and C_2 at sea level) and 32 potential electrodes (P_1, P_2, . . ., P_{32}) installed in one multiconductor electrode array cable with two depth meters and a sea anchor. The transmitter and receiver are loaded on the rear deck of the survey boat.

Instruments and field experiment

To evaluate the performance and efficiency of the proposed VEC-DC system, we carried out field experiments at the Shimizu Port in Suruga Bay, Japan (Figure 1). For VEC-DC data acquisition in the field, we developed a new measurement system that operates in seawater to depths of 30 to 100 m. The new VEC-DC system consists of four primary components: (a) a DC transmitter and datalogger, (b) an electrode array cable for potential measurement, (c) two single-conductor cables for the current injection, and (d) two water-depth meters (Figures 2 and 3). The potential electrode array cable consists of 32 single conductor cables with stainless steel electrodes (P_1 to P_{32}, Figure 3). This is deployed vertically from the rear deck of the survey boat with a single current electrode (C_1) cable, two depth meters, and a sea anchor attached with rope (Figure 2). Another current electrode (C_2) is deployed at sea level with a buoy, which is kept 30 to 50 m away from the front of the survey boat (Figure 2). For the transmitter and receiver mounted on the survey boat, we adopted a commercial onshore DC resistivity survey system (McOHM Profiler4 by OYO) to yield transmitting currents and measure electric potentials. The specification of each component is shown in Table 1. Measurements were conducted at two sites around the Shimizu Port in Suruga Bay. These are denoted as #01 and #02 (sea depths of approximately 45 and 60 m, respectively) in Figure 1. At the measurement sites, the electrode array cable of potential measurement (P_1 to P_{32}) and single-conductor cable for the seafloor current electrode (C_1) were deployed from the survey boat. Two small depth meters (MDS-MkV/D, JFE Advantec, Kobe, Hyogo Prefecture, Japan) were attached to the rope. One was fixed to the end that was lowered to the seafloor, and the other was fixed 10 m above the first one to estimate the depth of the electrodes and the tilt angle of the

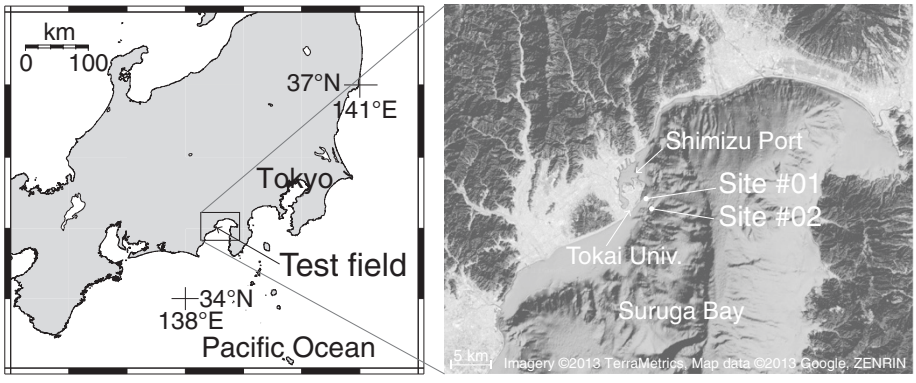

Figure 1 Map of the field experiment. Map of the field experiment area and locations of test sites.

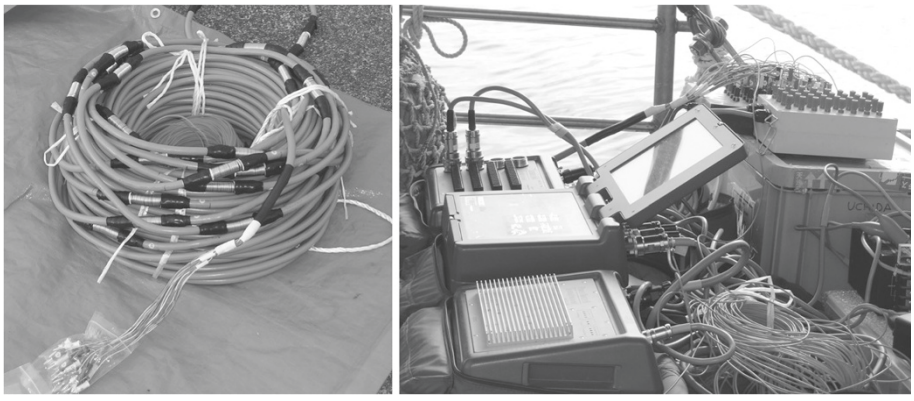

Figure 3 Photo of instruments. Electrode array cable for electric potential measurement (left) and DC measurement instruments (McOHM Profiler4) on the survey boat (right).

cables during the measurements. We used 0.5 and 1.0 m electrode spacings at the two measurement sites. Each measurement recorded 31 pairs (channels) of potential differences ΔV, given by

$$\Delta V_i = \phi(\mathrm{P}_i) - \phi(\mathrm{P}_{i+1}),\ i = 1, \ldots, 31, \tag{1}$$

using 32 potential electrodes. The current electrodes were fixed at the seafloor (C_1) and at sea level (C_2). The data acquisition time depends on the choice of data stacking number of the McOHM Profiler4; it generally took 1 to 10 min to measure 31 potential differences. After several data acquisition runs with different stacking numbers, the rope, current electrode cable, and electrode array cable were retrieved. Figure 4a,b shows the observed electric potential difference ΔV using the VEC-DC system at test sites #01 and #02, respectively. Each data set contains a total of 31 voltages ($\Delta V_i, i = 1, 2, \ldots, 31$) measured at 32 potential electrodes for the two fixed current electrodes described above. The results show that high-quality data were obtained at both sites, down to approximately 1×10^{-4} V (0.1 mV). This implies that the VEC-DC system and survey configuration of this experiment has a noise level of approximately 0.1 mV. The maximum tilt angle of the electrode cables, estimated from the two depth meter logs, was less than 1.5°, so we assume that the cables retained their vertical position during data acquisition.

Numerical analysis

Electric potential and apparent resistivity

In this study, we perform one-dimensional (1D) numerical analysis with a multilayered space including seawater and sub-seafloor layers. We begin by formulating the electric potential and introducing an apparent resistivity for the marine VEC-DC method. We then develop a 1D inversion method using simulated annealing (SA) for the VEC-DC data and finally apply this inversion method to the field data.

The formula for the electric potential generated by a point current source placed at any position (except layer interfaces) in a multilayered space has been given using cylindrical coordinates by Mitsuhata and Ueda (2010), as shown in Figure 5. In this section, we present a summary

Table 1 Specification of the VEC-DC system

Transmitter, receiver, and scanner	McOHM Profiler4 (OYO)
Current	1A, 1 Hz
Potential electrode cable	Water-resistant 32-channel electrode array cable
	0.3 $mm^2 \times$ 100 m $\times$ 32.20 kg
Potential electrode	ϕ1.4 mm stainless steel 2.0 m (multiple turn with 50 mm)
Potential electrode spacing	0.5 and 1.0 m
Current electrode cable	0.5 $mm^2 \times$ 100 m $\times$2
Current electrode	ϕ16 mm $\times$ 200 mm stainless steel $\times$2
Depth meter	MDS-MkV/D (JFE Advantec)
	ϕ18 mm $\times$ 93 mm (resolution, 0.05 m)
Sea anchor	10 kg

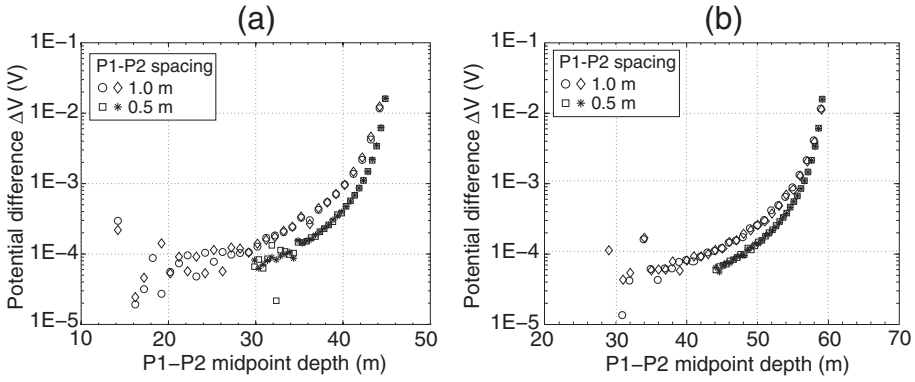

Figure 4 Observed data. Observed data (electric potential difference) at the test sites **(a)** #01, sea depth 45 m and **(b)** #02, sea depth 60 m.

of the formula given in Mitsuhata and Ueda (2010). In the cylindrical coordinate system, the governing equation for the electric potential ϕ_i given by the source $(0, z_c)$ at receiver (r, z) in the ith layer is described as

$$\frac{\partial^2 \phi_i}{\partial r^2} + \frac{1}{r}\frac{\partial \phi_i}{\partial r} + \frac{\partial^2 \phi_i}{\partial z^2} = 0, \tag{2}$$

where r is the horizontal distance between the source and the receiver. The general solution ϕ_i of (2) is given by a Hankel transform using the coefficients D, U, and Bessel's function (e.g., Koefoed 1979; Zhdanov and Keller 1994).

$$\phi_i = \frac{I}{4\pi}\int_0^\infty \left(U_i e^{\lambda(z-z_i)} + D_i e^{-\lambda(z-z_i)}\right) J_0(\lambda r)\, d\lambda. \tag{3}$$

The potential ϕ_i is determined by coefficients U_i and D_i. Details of the solution of (3) are shown in Mitsuhata and Ueda (2010) and Ueda et al. (2010). A digital filter is generally used to compute the Hankel transforms in (3) (e.g., Anderson 1979; Guptasarma and Singh 1997; Rijo and Almeida 2003). In our calculation code (Ueda et al. 2010), we adopt the digital filters provided by Rijo and Almeida (2003). It is common to introduce the apparent resistivity

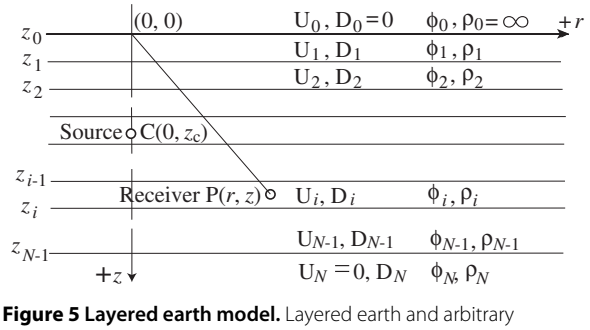

Figure 5 Layered earth model. Layered earth and arbitrary electrode location model presented by Mitsuhata and Ueda 2010 and Ueda et al. 2010.

instead of the electric potential for the initial estimation of subsurface resistivity distribution (e.g., Koefoed 1979; Zhdanov and Keller 1994). In marine/underwater electrical methods, the apparent resistivity can be defined as, for example, (1) ρ_a for the whole space model, and (2) ρ_s in the double half-space with a seawater resistivity of ρ_w (e.g., Francis 1985; Jones 1999, p. 255). For the whole space with resistivity ρ_a, the electric potential difference (ΔV) of a four-electrode configuration (Figure 6a) is given by

$$\Delta V = \rho_a I\,(4\pi r)^{-1} \text{ and } \rho_a = I^{-1}\,(4\pi r \Delta V), \tag{4}$$

where r is a function of the distance between current and potential electrodes, defined as $r^{-1} = r_{11}^{-1} + r_{22}^{-1} - r_{21}^{-1} - r_{12}^{-1}$. For the double half-space (e.g., seawater ρ_w and seafloor ρ_s, shown in panel b of Figure 6), ΔV for a four-electrode configuration is obtained by the method of images (e.g., Reynolds 1997):

$$\Delta V = \rho_w I\,(4\pi)^{-1}\left(r^{-1} + k r'^{-1}\right), \tag{5}$$

where k is an electrical reflection coefficient defined as

$$k = (\rho_s - \rho_w)\,/\,(\rho_s + \rho_w) \tag{6}$$

and $r'^{-1} = r'^{-1}_{11} + r'^{-1}_{22} + r'^{-1}_{21} + r'^{-1}_{12}$. Therefore, by solving for ΔV using (4) and (5), ρ_s is obtained as

$$\rho_s = \left\{\rho_w^2\left(r' - r\right) - r'\rho_w\rho_a\right\} \Big/ \left\{r'\rho_a - \rho_w\left(r' + r\right)\right\}. \tag{7}$$

For multilayered and/or multidimensional sub-seafloor regions, ρ_s represents the apparent resistivity of the entire sub-seafloor domain.

Very fast simulated annealing for VEC-DC data

For the data inversion, we adopt a very fast simulated annealing (VFSA, e.g., Sharma 2012) optimization, which is based on the simulated annealing (SA) algorithm (e.g., Sen et al. 1993). In this study, we simply follow the VFSA algorithm presented by Sharma (2012) and implement the one-dimensional inversion computer code for VEC-DC

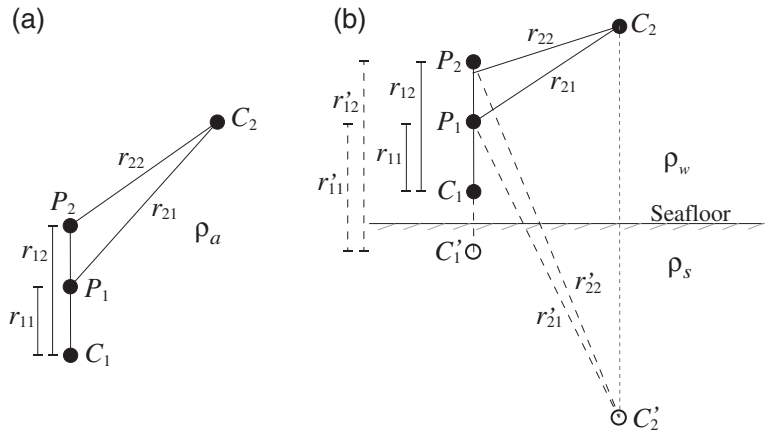

Figure 6 Schematic illustration of the whole space and two half-space models. Schematic illustration of the whole space and two half-space models with four electrodes (after Ueda et al. 2010). **(a)** A VEC-DC four-electrode configuration where the current and potential electrodes are placed in the whole space of resistivity ρ_a. **(b)** A four-electrode configuration for the double half-space model. In **(b)**, ρ_w denotes seawater resistivity and ρ_s represents sub-seafloor resistivity. Electrodes *C* and *P* represent current and potential electrodes, respectively, with black circles. Electrode *C*′ (open circle) denotes the image source of the current electrode *C* due to the seafloor.

data in MATLAB. The unknown model parameters of the VFSA inversion are represented by model *P* and include ρ and *h*, the resistivity and thickness of sub-seafloor layers, respectively. Observed electric potentials are converted to the seafloor apparent resistivity ρ_s using ρ_w, (4), and (7). Model parameter *P* and data ρ_s are transformed into the log domain. Then, following Sharma (2012), the objective function ε is defined as

$$\varepsilon = \frac{1}{N}\sum_{j=1}^{N}\left\{\ln\left(\rho_{sj}^{\mathrm{Obs}}\right) - \ln\left(\rho_{sj}^{\mathrm{Prd}}(P)\right)\right\}^2, \tag{8}$$

where ρ_{sj}^{Obs} and $\rho_{sj}^{\mathrm{Prd}}(P)$ are the *j*th observed and predicted (computed with estimated model *P*) data, respectively. *N* is the number of data (a total of 31 data points for the current VEC-DC system). During the VFSA inversion, model parameters P_i^m for the *m*th iteration are updated to P_i^{m+1} according to

$$P_i^{m+1} = P_i^m + y_i\left(P_i^{\max} - P_i^{\min}\right), \tag{9}$$

where $P_i^{\max}$ and $P_i^{\min}$ are upper and lower bounds of the *i*th model parameter P_i and y_i is the updating factor computed as

$$y_i = \mathrm{sgn}\,(u_i - 0.5)\,T_m\left\{\left(1 + T_m^{-1}\right)^{|2u_i-1|} - 1\right\}. \tag{10}$$

Here, $u_i \in [0,1]$ is a random number, and T_m is the temperature,

$$T_m = T_0 exp\left(-cm^{\alpha}\right), \tag{11}$$

which controls the convergence behavior of the VFSA inversion. The variable *m* is the iteration number, *c* and α are constant parameters, and T_0 is the initial temperature. In this study, we use $c = 1$ and $\alpha = 0.5$. The number of temperature cooling steps is fixed to 100, and at each temperature, the update calculation (9) is repeated (20 × number of unknown model parameters) times to yield a better solution. Therefore, the total number of SA iterations (model evaluation) is 100 × 20 × (number of unknown model parameters) (e.g., a total of 6,000 iterations for two layers with three unknown parameters). Details of the VFSA inversion algorithm and parameters used in this study are available in Sharma (2012). We have developed the VFSA inversion code based on the VFSA algorithm described above. This was applied to the synthetic data generated by a test model to verify that appropriate results had been obtained. Figure 7

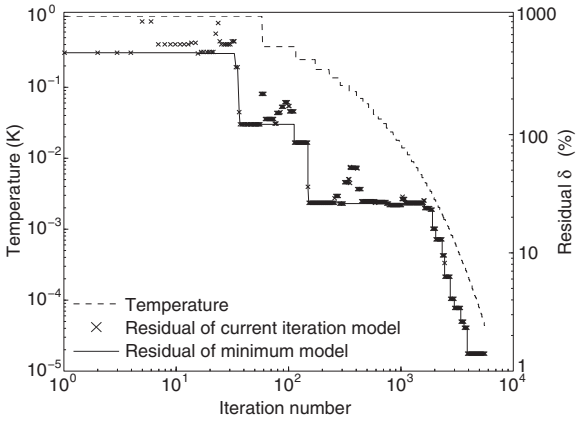

Figure 7 Plot of the residual. Plot of the residual of current and minimum models depending on number of iterations in the VFSA inversion of synthetic VEC-DC data. Dashed line represents temperature cooling and crosses and solid lines show residuals of the current and minimum models, respectively.

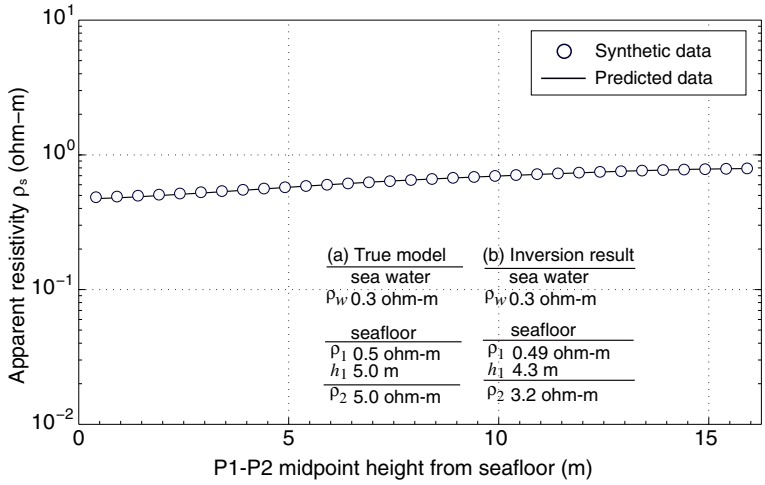

Figure 8 Comparison of synthetic data and predicted data. Comparison of synthetic data and predicted data computed from the VFSA inversion model.

shows the VFSA convergence behavior for the synthetic VEC-DC data. Figure 8 presents the synthetic data and predicted apparent resistivity obtained by the VFSA inversion as a function of the distance of the electrodes from the seafloor. In this verification, a sub-seafloor model consists of two layers, and the unknown model parameters are (ρ_1, h_1, and ρ_2).

The synthetic true model has $\rho_1 = 0.5\ \Omega\cdot$ m, $h_1 = 5.0$ m, and $\rho_2 = 5.0\ \Omega\cdot$m, while the SA inversion results are $\rho_1 = 0.49\ \Omega\cdot$m, $h_1 = 3.2$ m, and $\rho_2 = 4.3\ \Omega\cdot$m.

The difference between (synthetic) observed and predicted data is defined as the residual δ (%),

$$\delta = \sqrt{\frac{1}{N}\sum_{j=1}^{N}\left(\frac{\ln \rho_{sj}^{\mathrm{Prd}}\ (P) - \ln \rho_{sj}^{\mathrm{Obs}}}{\ln \rho_{sj}^{\mathrm{Obs}}}\right)^2} \times 100\ \ (\%). \tag{12}$$

The fit between observed and predicted data appears to be good, and the resulting residual of the inversion is 1.47%. Thus, we can apply the developed SA inversion technique to the VEC-DC data.

Field data inversion

Next, we applied the proposed SA inversion to the real VEC-DC data collected at Shimizu Port. In this inversion, we assume a model consisting of a uniform seawater layer and (a) a uniform sub-seafloor and (b) two sub-seafloor layers. The unknown model parameters for the VFSA optimization are the sub-seafloor resistivity ρ_1 for the uniform sub-seafloor model, the sub-seafloor resistivities ρ_1, ρ_2, and the first sub-seafloor layer's thickness h_1, for the two sub-seafloor layer model. The seawater layer resistivity and thickness are fixed to 0.3 $\Omega\cdot$m and 60 m, respectively, during the VFSA procedure. The resulting two sub-seafloor layer model at site #01 has $\rho_1 = 0.11\ \Omega\cdot$m, $\rho_2 = 0.89\ \Omega\cdot$m, and $h_1 = 0.55$ m, while that for site #02 gives $\rho_1 = 0.13\ \Omega\cdot$m, $\rho_2 = 0.78\ \Omega\cdot$m, and $h_1 = 0.8$ m. Figure 9 presents the VFSA convergence behavior for the field VEC-DC data. Figure 10 plots the observed data and predicted apparent resistivity obtained by the VFSA inversion depending on the heights of the electrodes from the seafloor. In Figure 10, the predicted data obtained by the VFSA inversion for a uniform sub-seafloor model with resistivity of 0.44 and 0.40 $\Omega\cdot$m for sites #01 and #02 are also presented. At site #01, the VFSA iteration converged with minimum residuals δ of 10.7% and 28.2% for

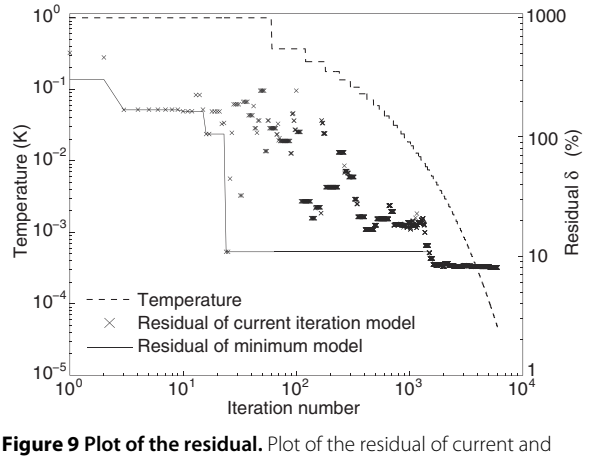

Figure 9 Plot of the residual. Plot of the residual of current and minimum models depending on number of iterations in the VFSA inversion of VEC-DC field data. Dashed line represents temperature cooling and crosses and solid lines show residuals of the current and minimum models, respectively.

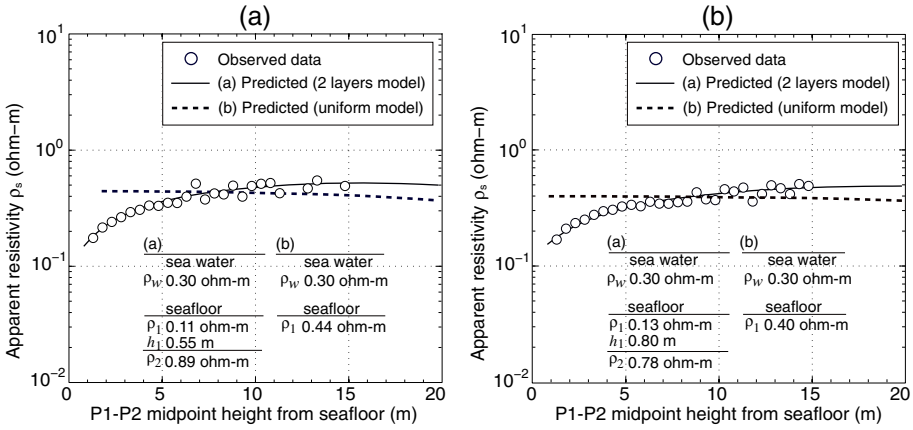

Figure 10 Comparison of observed data and predicted data. Comparison of observed data and predicted data computed from the VFSA inversion model for test sites **(a)** #01 and **(b)** #02.

the two-layer and uniform model, respectively. At site #02, the results gave 8.0% and 23.4% for the two-layer and uniform model, respectively. It can be clearly seen that the predicted data for the two sub-seafloor layer model fits the observed data better than those for the uniform sub-seafloor model at both sites. These results indicate that both sub-seafloor resistivity mapping and sounding information could be obtained by the VEC-DC measurements. Considering the noise level (0.1 mV) and transmitting current (1 A) of the proposed VEC-DC system, it is necessary to increase the transmitting current for deep resistivity sensing.

Conclusion

We have developed a vertical electrode configuration DC measurement method and reported the results of field experiments in a shallow water coastal zone. We conducted field experiments to evaluate the performance and efficiency of the proposed system in the shallow water zone around Shimizu Port, Suruga Bay, Japan. To interpret the VEC-DC data, we adopted theoretical formulas and computed the electric potential generated by a point current source placed at any position within an arbitrary electrode configuration in a multilayered space including seawater and sub-seafloor regions. An inversion method for VEC-DC data was also developed. This is based on VFSA optimization and was applied to the synthetic and actual data obtained from the field experiments. The observed data were of good quality, except for those below the system noise level. A resistivity model with two sub-seafloor layers was estimated by the VFSA inversion. The results confirm that the VEC-DC method can be applied to sub-seafloor resistivity mapping as well as for vertical resistivity sounding.

The positions and locations of vertically deployed electrodes can be determined with two small depth meters, meaning there is no need for large-scale underwater positioning systems, such as an acoustic pinger and GPS buoy. This makes the VEC-DC field operation simple and the system compact, easily handled with a small boat. It would be suitable for efficient near-seafloor resistivity mapping in rugged seafloor environments where it would be difficult to measure the exact positions and locations of individual electrodes in a horizontal electrode configuration (HEC) without any sophisticated positioning devices. It is important to understand the advantages and disadvantages of both VEC and HEC and to choose the right method depending on individual targets and situations.

In future studies, we will focus on improving our VEC-DC method for deeper resistivity sounding and applying it to the exploration of various targets.

Abbreviations

DC: direct current; HEC: horizontal electrode configuration; VEC: vertical electrode configuration.

Competing interests

The authors declare that they have no competing interests.

Authors' contributions

TU designed the study and instrumentation, developed the numerical methods, participated in the field experiment, conducted the numerical analysis and interpretation, and drafted the manuscript. YM carried out the theoretical formulation, participated in the numerical analysis and interpretation, and helped to draft the manuscript. MJ participated in the survey design and the field experiment. HB organized the field experiment and participated in the field measurements. All authors read and approved the final manuscript.

Acknowledgements

The authors would like to thank the survey crew of Minami-Juuji for their assistance with VEC-DC data acquisition. We also acknowledge Mr. M. Inoue for his advice and suggestions regarding marine/underwater DC resistivity measurements, including field surveys and data interpretation. We would also like to thank the two anonymous reviewers for their valuable comments and contributions to this letter.

Author details
[1]Geological Survey of Japan, AIST, Central 7, 1-1-1, Higashi, Tsukuba 305-8567, Japan. [2]School of Marine Science and Technology, Tokai University, 3-20-1, Orido, Shimizu-ku, Shizuoka 424-8610, Japan.

Received: 8 November 2013 Accepted: 1 April 2014
Published: 6 May 2014

References

Anderson WL (1979) Numerical integration of related Hankel transforms of orders 0 and 1 by adaptive digital filtering. Geophysics 44: 1287–1305
Baumgartner F (1996) A new method for geoelectrical investigations underwater. Geophys Prospect 44: 71–98
Barsukov P, Fainberg EB, Singer BS (2007) A method for hydrocarbon reservoir mapping and apparatus for use when performing the method. International Patent WO 2007/053025, 10 May 2007
Chave AD, Constable SC, Edwards RN (1991) Electrical exploration methods for the seafloor. Electromagn Methods Appl Geophys Vol. 2, Appl Parts A B 2: 931–966
Constable SC (2010) Ten years of marine CSEM for hydrocarbon exploration. Geophysics 75(5): 75A67–75A81
Edwards RN, Law KL, Wolfgram PA, Nobes DC, Bonet MN, Trigg DF, Delauriert JM (1985) First results of the MOSES experiment: sea sediment conductivity and thickness determination, Bute Inlet, British Columbia, by magnetometric offshore electrical sounding. Geophysics 50: 153–161
Francis TJG (1985) Resistivity measurements of an ocean floor sulphide mineral deposit from the submersible Cyana. Mar Geophys Res 7: 419–437
Goto T, Takafumi K, Hideaki M, Ryo T, Ryo M, Yoshihisa O, Mikio S, Toshiki W, Nobukazu S, Hitoshi M, Yoshinori S, Masataka K (2008) A marine deep-towed DC resistivity survey in a methane hydrate area, Japan Sea. Explor Geophys 39: 52–59
Guptasarma D, and Singh B (1997) New digital linear filters for Hankel J0 and J1 transforms. Geophys Prospect 45(5): 745–762
Holten T, Flekkøy EG, Singer B, Blixt EM, Hanssen A, and Måløy KJ (2009) Vertical source, vertical receiver, electromagnetic technique for offshore hydrocarbon exploration. First Break 27: 89–93
Jones EJW (1999) Marine geophysics. John Wiley & Sons, LTD, New York, p 255
Koefoed O (1979) Geosounding principles. vol. 1: resistivity sounding measurements. Elsevier, Amsterdam
Loke MH, Lane JW (2004) Inversion of data from electrical resistivity imaging surveys in water-covered areas. Explor Geophys 35(4): 266–271
Mitsuhata Y, Ueda T (2010) Direct current electric potentials for a multilayered earth with arbitrary electrode configurations: derivation of theoretical recurrence formulas for a point current source excitation (in Japanese). BUTSURI-TANSA (Geophys Exploration) 63(2): 197–208
Orlando L (2013) Some considerations on electrical resistivity imaging for characterization of waterbed sediments. J Appl Geophys 95: 77–89
Reynolds JM (1997) An introduction to applied and environmental geophysics. In: Geophysics, vol 1. John Wiley & Sons, LTD, New York, pp 434–436
Rijo L, Almeida FL (2003) New optimized digital filters for sine, co-sine J0 and J1 Hankel transforms. In: 8th Int. Congr. Bras. Geophys. Soc. Brazilian Geophysical Society, pp 1–6
Sato HK (2000) Potential field from a dc current source arbitrarily located in a nonuniform layered medium. Geophyics 65(6): 1726–1732
Sen MK, Bhattacharya BB, Stoffa PL (1993) Nonlinear inversion of resistivity sounding data. Geophysics 58(4): 496–507
Sharma SP (2012) VFSARES-a very fast simulated annealing FORTRAN program for interpretation of 1-D DC resistivity sounding data from various electrode arrays. Comput Geosci 42: 177–188
Ueda T, Mitsuhata Y, Uchida T (2010) Direct current electric potentials for a multilayered earth with arbitrary electrode configurations: numerical methods and simulation of marine resistivity exploration (in Japanese). BUTSURI-TANSA (Geophys Exploration) 63(3): 229–238
Zhdanov MS, Keller GV (1994) The geoelectrical methods in geophysical exploration. Elsevier, Amsterdam

doi:10.1186/1880-5981-66-31
Cite this article as: Ueda *et al.*: Sub-seafloor resistivity sensing using a vertical electrode configuration. *Earth, Planets and Space* 2014 **66**:31.